Large G protein α-subunit XLαs limits clathrin-mediated endocytosis and regulates tissue iron levels in vivo

Qing He[a], Richard Bouley[b], Zun Liu[a], Marc N. Wein[a], Yan Zhu[a], Jordan M. Spatz[a], Chia-Yu Wang[b], Paola Divieti Pajevic[a,c], Antonius Plagge[d], Jodie L. Babitt[b], and Murat Bastepe[a,1]

[a]Endocrine Unit, Department of Medicine, Massachusetts General Hospital and Harvard Medical School, Boston, MA 02114; [b]Program in Membrane Biology, Department of Medicine and Division of Nephrology, Massachusetts General Hospital and Harvard Medical School, Boston, MA 02114; [c]Department of Molecular and Cell Biology, Boston University Henry M. Goldman School of Dental Medicine, Boston, MA 02118; and [d]Department of Cellular and Molecular Physiology, Institute of Translational Medicine University of Liverpool, Liverpool L69 3BX, United Kingdom

Edited by Robert J. Lefkowitz, Howard Hughes Medical Institute, Duke University Medical Center, Durham, NC, and approved September 28, 2017 (received for review July 19, 2017)

Alterations in the activity/levels of the extralarge G protein α-subunit (XLαs) are implicated in various human disorders, such as perinatal growth retardation. Encoded by *GNAS*, XLαs is partly identical to the α-subunit of the stimulatory G protein (Gsα), but the cellular actions of XLαs remain poorly defined. Following an initial proteomic screen, we identified sorting nexin-9 (SNX9) and dynamins, key components of clathrin-mediated endocytosis, as binding partners of XLαs. Overexpression of XLαs in HEK293 cells inhibited internalization of transferrin, a process that depends on clathrin-mediated endocytosis, while its ablation by CRISPR/Cas9 in an osteocyte-like cell line (Ocy454) enhanced it. Similarly, primary cardiomyocytes derived from XLαs knockout (XLKO) pups showed enhanced transferrin internalization. Early postnatal XLKO mice showed a significantly higher degree of cardiac iron uptake than wild-type littermates following iron dextran injection. In XLKO neonates, iron and ferritin levels were elevated in heart and skeletal muscle, where XLαs is normally expressed abundantly. XLKO heart and skeletal muscle, as well as XLKO Ocy454 cells, showed elevated SNX9 protein levels, and siRNA-mediated knockdown of SNX9 in XLKO Ocy454 cells prevented enhanced transferrin internalization. In transfected cells, XLαs also inhibited internalization of the parathyroid hormone and type 2 vasopressin receptors. Internalization of transferrin and these G protein-coupled receptors was also inhibited in cells expressing an XLαs mutant missing the Gα portion, but not Gsα or an N-terminally truncated XLαs mutant unable to interact with SNX9 or dynamin. Thus, XLαs restricts clathrin-mediated endocytosis and plays a critical role in iron/transferrin uptake in vivo.

heterotrimeric G proteins | stimulatory G protein | GNAS | endocytosis | transferrin

Endocytosis is a fundamental cellular process by which fluid or particles from the extracellular space or different macromolecules of the plasma membrane are internalized into transport vesicles (1–4). It thus plays a role in a wide variety of cellular and physiological functions, including signal transduction, neurotransmission, and development. Mutations in the genes encoding some of the core components of endocytosis cause human diseases, such as familial hypocalciuric hypocalcemia (5), certain types of Charcot-Marie-Tooth disease (6), centronuclear myopathy (7), and late-onset Alzheimer's disease (8). Moreover, the pathogenesis of certain neurodegenerative diseases critically involves endocytosis and related cellular processes (9). In addition, intracellular targeting of many clinical drugs relies on the endocytic pathway (10). Endocytosis is tightly regulated and involves coordinated actions of a range of proteins at the plasma membrane.

Signals from many hormones, neurotransmitters, and autocrine/paracrine factors are transduced at the plasma membrane via the action of the stimulatory heterotrimeric G protein (11, 12). The α-subunit of this ubiquitously expressed protein (Gsα) is encoded by the *GNAS* complex locus, mutations of which are responsible for multiple human diseases that affect a variety of organ systems (13, 14). *GNAS* also gives rise to a large Gsα variant termed extralarge G protein α-subunit (XLαs) (15). Derived from an upstream, paternally active promoter, XLαs uses a separate first exon that splices onto exons 2–13 used by Gsα. XLαs is thus partly identical to Gsα and comprises most functional domains of the latter (16). However, XLαs and Gsα differ markedly in their amino-terminal domains. Loss or gain of XLαs activity is thought to contribute directly to some of the phenotypes resulting from *GNAS* alterations, including intrauterine growth retardation seen frequently in patients with pseudopseudohypoparathyroidism, progressive ossesous heteroplasia, platelet Gs-hypofunction abnormalities, and certain types of breast cancers (17–20). Nevertheless, the cellular actions of XLαs, unlike the actions of Gsα, have remained poorly defined.

XLαs shows strong plasma membrane avidity and, unlike Gsα, remains anchored to the plasma membrane following activation by G protein-coupled receptors (GPCRs) or GTPase inhibiting mutations (21, 22). The unique amino-terminal domain of XLαs (XL domain) is larger than and differs markedly from that of Gsα. The XL domain contains multiple proline-rich motifs, suggesting that this domain may be involved in functionally

Significance

Mutations in the gene encoding XLαs and Gsα (*GNAS*) cause several genetic diseases and various tumors. Although alterations in XLαs activity/levels are implicated in some of these disorders, cellular actions of XLαs have remained poorly defined. We identified dynamins and sorting nexin-9, key components of clathrin-mediated endocytosis, as binding partners of XLαs and showed that XLαs, but not Gsα, restricts clathrin-mediated endocytosis and plays a role in iron/transferrin uptake in vivo. Thus, impaired or enhanced endocytosis may be involved in the pathogenesis of some of the *GNAS*-related diseases. Our findings also provide insights into the roles of heterotrimeric G proteins and the mechanisms underlying endocytosis, a fundamental cellular process required for nutrient uptake and regulation of cell signaling.

Author contributions: Q.H., J.L.B., and M.B. designed research; Q.H., R.B., Z.L., M.N.W., and Y.Z. performed research; J.M.S., C.-Y.W., P.D.P., and A.P. contributed new reagents/analytic tools; Q.H., R.B., Z.L., M.N.W., Y.Z., C.-Y.W., J.L.B., and M.B. analyzed data; and Q.H. and M.B. wrote the paper.

The authors declare no conflict of interest.

This article is a PNAS Direct Submission.

[1]To whom correspondence should be addressed. Email: bastepe@helix.mgh.harvard.edu.

This article contains supporting information online at www.pnas.org/lookup/suppl/doi:10.1073/pnas.1712670114/-/DCSupplemental.

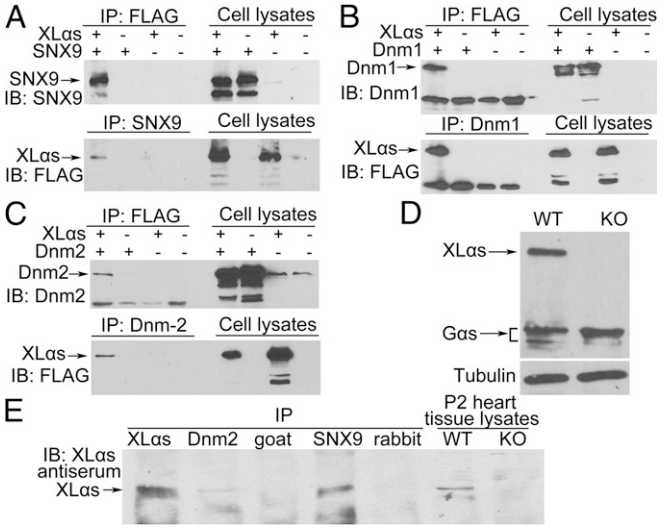

Fig. 1. XLαs can be coimmunoprecipitated with SNX9, Dnm1, and Dnm2. (*A*–*C*) XLαs-FLAG was coexpressed with (*A*) SNX9, (*B*) Dnm1, or (*C*) Dnm2 in HEK293T cells. Cells transfected with pcDNA plasmid were used as control. Total cell extracts were immunoprecipitated with (*A*) anti-SNX9, (*B*) anti-Dnm1, (*C*) anti-Dnm2 or anti-FLAG antibodies. The immunoprecipitated proteins were analyzed subsequently by immunoblot using anti-FLAG or (*A*) anti-SNX9, (*B*) anti-Dnm1, or (*C*) anti-Dnm2 antibodies. (*D*) Protein lysates from P2 WT and XLKO hearts were immunoblotted with a Gsα antibody recognizing both XLαs and Gsα. (*E*) Heart tissue lysates from P2 WT mice were immunoprecipitated with anti-XLαs, anti-Dnm2, or anti-SNX9 antibodies, and then, immunoblot was performed using XLαs antiserum. Goat IgG and the rabbit IgG served as negative controls for immunoprecipitation. Heart tissue lysates from P2 WT and XLKO mice were used for immunoblotting to identify the specific XLαs band. These results are representative of at least three independent experiments.

important interactions at the plasma membrane. In this study, we aimed to discover the unique cellular actions of XLαs by identifying protein–protein interactions involving this protein. We revealed two proteins important for endocytosis, sorting nexin-9 (SNX9) and dynamin (Dnm), as binding partners of XLαs. Our subsequent studies showed that XLαs plays an inhibitory role in endocytosis and regulates iron/transferrin uptake.

Results

XLαs Forms Complexes with SNX9, Dnm1, and Dnm2. To identify binding partners of XLαs, we performed an initial proteomic screen whereby lysates of C3H10T1/2 cells (a mouse cell line functionally similar to mesenchymal stem cells) overexpressing FLAG-tagged XLαs or YFP were purified on an anti-FLAG affinity resin, followed by LC-MS/MS. As expected, copurified proteins identified selectively from XLαs-expressing cells included some G protein subunits, as well as alternative gene product encoded by the XL exon (ALEX), which is known to interact with XLαs (23) (*SI Appendix*, Table S1). This screen identified SNX9, a SH3 domain-containing protein critical for endocytosis (24), as a binding partner of XLαs. The screen also identified Dnm1 and Dnm2, which interact with SNX9 and are also critical for endocytosis (24, 25).

To verify these interactions, we performed coimmunoprecipitation experiments. FLAG-XLαs, SNX9, or both were overexpressed in HEK293T cells and immunoprecipitated from total cell lysates using anti-FLAG antibody. Subsequent immunoblots using anti-SNX9 antibody detected SNX9 only in samples from cells coexpressing XLαs and SNX9 (Fig. 1*A*). Conversely, the lysates were immunoprecipitated by anti-SNX9 antibody, and coimmunoprecipitated proteins were analyzed by immunoblots using anti-FLAG antibody. XLαs was successfully detected only in samples from cells coexpressing both XLαs and SNX9 (Fig. 1*A*). We also confirmed the XLαs–Dnm1 and XLαs–Dnm2 interactions by similar coimmunoprecipitation experiments using anti-Dnm1 or anti-Dnm2 antibodies (Fig. 1 *B* and *C*).

Abundant XLαs mRNA expression has been found by Northern blots in early postnatal mouse heart (26). Western blots using a C-terminal Gsα antibody, which could recognize both Gsα and XLαs, confirmed that XLαs was abundantly expressed in heart at postnatal day 2 (P2), and that its expression was absent in heart from XLαs knockout (XLKO) mice (Fig. 1*D*). To determine whether interactions between XLαs and SNX9/dynamins take place at physiological levels in vivo, we thus used protein lysates of hearts from P2 wild-type (WT) mice, or skeletal muscle from neonates. The lysates were immunoprecipitated with anti-XLαs, anti-Dnm2, or anti-SNX9 antibodies, and goat and rabbit IgG were used as controls. Western blot analysis of the immunoprecipitated proteins by using anti-XLαs antiserum revealed coimmunoprecipitation of XLαs with SNX9 and Dnm2 (Fig. 1*E* and *SI Appendix*, Fig. S1).

XLαs Overexpression Inhibits Transferrin Receptor Internalization. Internalization of the transferrin receptor, by which transferrin-bound iron enters into cells, has been extensively studied as a prototype for clathrin-mediated endocytosis. To determine whether XLαs has a role in transferrin internalization, we transfected HEK293T cells with cDNA encoding GFP-tagged XLαs and treated these cells with transferrin-Alexa Fluor 568 for 30 min. Confocal microscopy showed that, while transferrin was internalized in untransfected cells, a much lower amount of transferrin-Alexa Fluor 568 was detected in cells overexpressing XLαs (Fig. 2*A*). We also

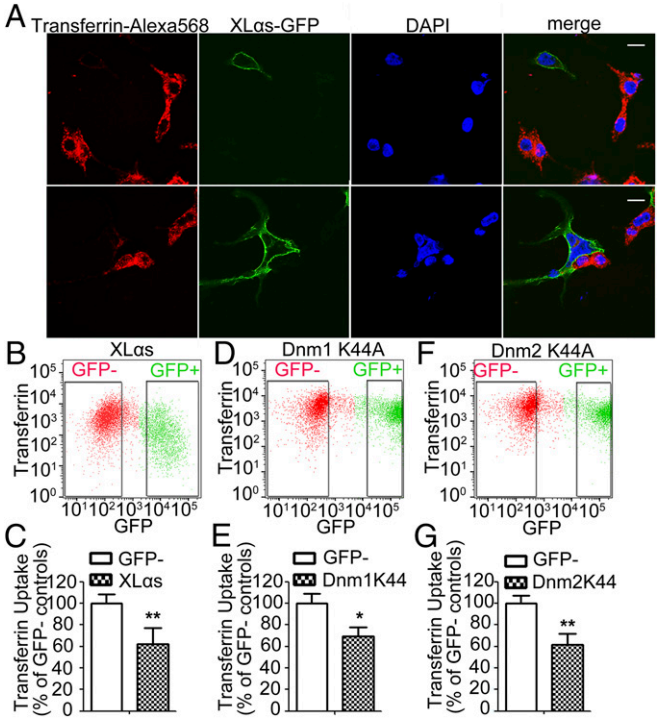

Fig. 2. XLαs represses TfRc internalization and transferrin uptake. (*A*) Confocal microscopy analysis of XLαs-GFP expressing cells incubated with transferrin-Alexa Fluor 568 (10 μg/mL) for 30 min. (Scale bar, 10 μm.) (*B*–*G*) Flow cytometry analysis of transferrin uptake in different transfected cells. Representative plots of transferrin uptake in cells transiently expressing (*B*) XLαs-GFP, (*D*) Dnm1 K44A-GFP, and (*F*) Dnm2 K44A-GFP. (*C*, *E*, and *G*) Quantification of the median values of transferrin-Alexa Fluor 568 in GFP^+ and GFP^- cell populations. Data are mean ± SEM of three independent experiments ($n = 12$ per group). $^*P < 0.05$, $^{**}P < 0.01$.

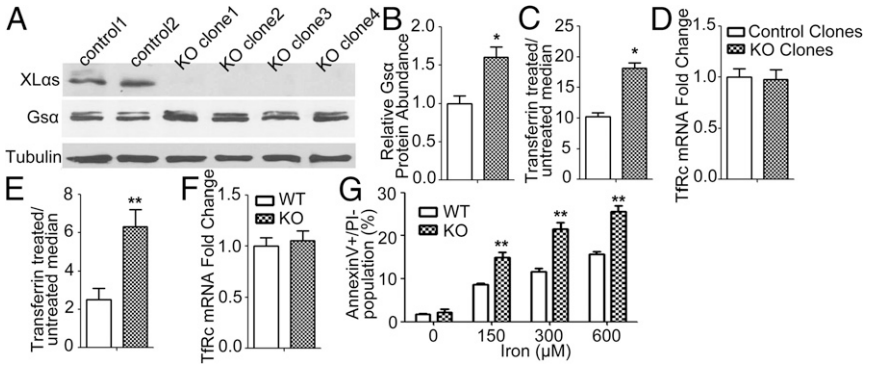

Fig. 3. Ablation of XLαs enhances transferrin uptake and iron overload-induced apoptosis. (*A*) Western blot analysis of XLαs and Gsα in clonal control and XLKO Ocy454 cells. (*B*) Densitometry analysis of Gsα immunoreactivity shown in *A*. (*C*) Ocy454 cells were untreated or treated with transferrin-Alexa Fluor 568 for 30 min, and then analyzed by flow cytometry for transferrin uptake for quantification of the median values of transferrin-Alexa Fluor 568 in treated and untreated cells. (*D*) TfRc mRNA expression levels in control and XLKO Ocy454 cells. qRT-PCR was performed by using β-actin as a reference control (n = 8 for control cells and n = 16 for XLKO cells from four independent expriments). (*E*) Transferrin uptake in primary cardiomyocytes from P2 WT and XLKO mice. Cells were untreated or treated with transferrin-Alexa Fluor 568 for 30 min and then analyzed by flow cytometry for the median values of transferrin uptake. (*F*) TfRc mRNA expression in primary cardiomyocytes. qRT-PCR was performed by using β-actin as a reference control (WT: n = 13; XLKO: n = 10 for primary cardiomyocytes isolated from three different litters). Data represent mean ± SEM *P < 0.05, **P < 0.01. (*G*) Primary cardiomyocytes from WT and KO mice were untreated or treated with $FeCl_3$ for 72 h, and the percentage of apoptotic cells was also analyzed by flow cytometric analysis of Annexin V/PI double staining. Results are expressed as the means ± SEM of four independent experiments (n = 18 in WT group; n = 14 in XLKO group). **P < 0.01 compared with control group.

performed flow cytometry to quantify transferrin uptake in untransfected and transfected cells. Cells overexpressing XLαs-GFP exhibited significantly lower transferrin uptake compared with untransfected cells (Fig. 2 *B* and *C*). As expected, dominant negative mutants of Dnm1 and Dnm2 (Dnm1-K44A and Dnm2-K44A) showed significant inhibition of transferrin endocytosis (Fig. 2 *D*–*G*).

Ablation of XLαs in Cultured Cells Promotes Transferrin Internalization. To further investigate the role of XLαs in transferrin uptake, we employed the osteocyte-like cell line Ocy454 cells (27, 28), since XLαs protein expression had been previously shown in bone (29). Using anti-XLαs antiserum we found that XLαs is expressed at readily detectable levels in Ocy454 cells (Fig. 3*A*). We ablated XLαs in these cells by using CRISPR/Cas9, and Western blots confirmed successful ablation of XLαs in four independent clonal cell lines (Fig. 3*A* and *SI Appendix*, Fig. S2 and Tables S2 and S3). Consistent with the findings in a previous report (30), Gsα protein levels in XLKO cells were modestly but significantly higher than in control cells (Fig. 3 *A* and *B*). The average level of transferrin uptake, as determined by 30-min treatment with transferrin-Alexa Fluor 568 followed by flow cytometry, was 1.8-fold higher in the XLKO clones than control cells (Fig. 3*C* and *SI Appendix*, Fig. S3*A*). Despite this increase in transferrin uptake, XLKO cells showed similar levels of mRNA encoding the transferrin receptor type 1 (TfRc) to control cells at baseline (Fig. 3*D*).

Loss of XLαs Is Associated with Enhanced Transferrin/Iron Uptake. To determine whether XLαs plays a physiological role in transferrin uptake, we cultured primary cardiomyocytes isolated from P2 WT and XLKO littermates. After treatment with transferrin-Alexa Fluor 568 for 30 min, followed by flow cytometry analysis, XLKO cardiomyocytes internalized 2.5-fold more transferrin compared with WT cardiomyocytes (Fig. 3*E* and *SI Appendix*, Fig. S3*B*). The baseline TfRc mRNA levels were comparable in XLKO and WT cells (Fig. 3*F*). Increased level of intracellular iron, which is mediated by transferrin internalization, leads to apoptosis (31–33). We treated primary cardiomyocytes isolated from P2 WT and XLKO pups with different concentrations of $FeCl_3$ for 72 h to induce iron overload. A significantly higher percentage of XLKO cells underwent apoptosis under different $FeCl_3$ concentrations compared with WT cells, as judged by the percentage of cells that are annexin V-positive and propidium iodide-negative (Fig. 3*G* and *SI Appendix*, Fig. S3*C*).

To examine whether the ablation of XLαs could increase iron uptake in vivo, we used XLKO mice and WT littermates and analyzed the cardiac tissue following iron dextran or vehicle injection for 10 d, starting from birth. Prussian blue staining of heart sections revealed more extensive myocardial iron accumulation in iron-injected XLKO pups than iron-injected WT pups (Fig. 4*A*). Diaminobenzidine (DAB)-enhanced Perl's staining of hearts from vehicle-injected mice also showed more extensive myocardial iron accumulation in P10 XLKO pups, indicating that the iron level in XLKO heart is elevated even in the absence of iron administration (Fig. 4*B*). Elevated tissue iron

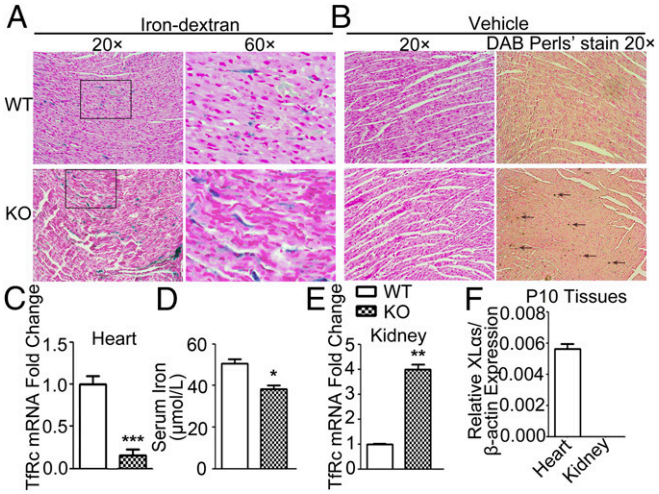

Fig. 4. P10 XLKO mice exhibit low serum iron levels with increased iron accumulation in heart. (*A*) Prussian blue staining of iron dextran-injected WT and XLKO mice shows more myocardial iron overload in XLKO samples. (*B*) DAB Perls' enhanced Prussian blue staining of vehicle-treated samples shows more iron deposition in XLKO samples at baseline. Arrows indicate positive stained cells. Images are representative of six to eight mice per genotype from four independent litters. (*C*) qRT-PCR analysis of TfRc using total RNAs isolated from P10 mouse hearts. (*D*) Serum iron levels in P10 WT and XLKO mice. (*E*) TfRc mRNA levels in P10 WT and XLKO kidneys. (*F*) qRT-PCR analysis of XLαs in P10 kidneys and hearts. qRT-PCR was performed by using β-actin as a reference control. Data represent mean ± SEM, *P < 0.05, **P < 0.01, ***P < 0.001; n = 9–12.

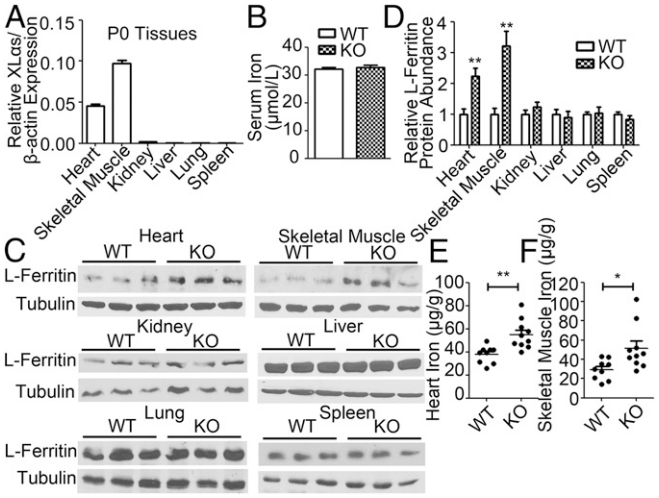

Fig. 5. XLKO neonates exhibit elevated L-ferritin expression and iron deposition in heart and skeletal muscle. (*A*) qRT-PCR analysis of XLαs in tissues from WT neonates (P0). (*B*) Serum iron levels in P0 WT and XLKO. (*C*) Protein lysates from P0 heart, skeletal muscle, kidney, liver, lung, and spleen were immunoblotted for L-ferritin antibody. α-Tubulin was used as loading control. (*D*) Densitometric analysis of the relative abundances of L-ferritin in different tissues. Data represent mean ± SEM of three independent measurements. (*E* and *F*) Iron content in (*E*) heart and (*F*) skeletal muscle. Mean and SEM are indicated as horizontal bars. $*P < 0.05$, $**P < 0.01$; $n = 9–12$.

levels are associated with decreased TfRc levels (34, 35). Accordingly, baseline TfRc mRNA levels were reduced markedly in XLKO hearts (Fig. 4*C*). In contrast, serum iron levels in P10 XLKO pups were significantly lower than in WT littermates (Fig. 4*D*) and consistent with serum iron deficiency, TfRc mRNA levels in kidney were elevated (Fig. 4*E*). qRT-PCR analysis demonstrated that, while XLαs mRNA was expressed abundantly in P10 heart, it was barely detectable in kidney (Fig. 4*F*). These results demonstrated that XLαs ablation increases iron levels in a tissue-specific manner. Together with data from cultured cells, these findings suggest that XLαs acts as an inhibitor of iron uptake.

XLKO Neonates Have Elevated Iron Levels in Heart and Skeletal Muscle. XLKO pups are slightly smaller than wild-type littermates at birth but otherwise display no gross abnormalities; however, these pups develop early postnatal growth retardation and disrupted glucose metabolism (26, 36). We thus analyzed XLKO neonates with respect to serum and tissue iron levels, focusing on tissues in which XLαs is either abundantly (e.g., heart and skeletal muscle) or poorly (kidney, liver, lung, and spleen) expressed (26, 37) (Fig. 5*A*). While serum iron levels were similar in newborn XLKO and WT pups (Fig. 5*B*), Western blot analyses showed that the levels of ferritin—an indicator of tissue iron status—in heart and skeletal muscle were significantly higher in XLKO neonates than in WT littermates (Fig. 5 *C* and *D*). In contrast, ferritin levels were similar in kidney, liver, lung, and spleen of XLKO and WT littermates (Fig. 5 *C* and *D*). Accordingly, iron content was significantly increased in neonatal XLKO heart and skeletal muscle (Fig. 5 *E* and *F*). These results were consistent with the above findings that XLαs inhibits transferrin/iron uptake and indicated a physiological role for XLαs as a negative regulator of tissue iron levels.

XLαs Ablation Increases SNX9 Levels, and SNX9 Knockdown Rescues the Enhanced Transferrin Uptake Observed in XLKO Ocy454 Cells. SNX9 levels are critical for mediating clathrin-mediated endocytosis (24, 38). Western blots showed that the level of SNX9 protein was significantly increased in P0 XLKO heart and skeletal muscle, but not in kidney, liver, lung, or spleen, compared with that in WT littermates (Fig. 6 *A* and *B*). The level of SNX9 protein was also elevated in XLKO Ocy454 cells compared with control cells (Fig. 6 *C* and *D*). Conversely, transient overexpression of XLαs in HEK293T cells resulted in a significant reduction in SNX9 protein levels (*SI Appendix*, Fig.S4). To examine the role of SNX9 in the action of XLαs, we knocked down SNX9 expression in both XLKO and control Ocy454 cells by using siRNA and confirmed the knockdown by Western blot analysis (Fig. 6 *C* and *D*). Diminished SNX9 expression resulted in a marked reduction of transferrin uptake in both XLKO and control Ocy454 cells, and essentially abrogated the enhanced transferrin uptake resulting from XLαs ablation (Fig. 6*E* and *SI Appendix*, Fig. S5).

The Proline-Rich N-Terminal Portion Is Required for the Inhibitory Effect of XLαs on Transferrin Uptake. SNX9 comprises a Src-homology 3 (SH3) domain, which plays an important role in its interaction with dynamins (24). SH3 domains interact with proline-rich motifs in other proteins (39). We thus examined whether SNX9 is able to interact with Gsα, which, unlike XLαs, lacks proline-rich motifs. We also constructed an N-terminally truncated XLαs mutant missing all proline-rich motifs and the highly conserved proline-rich region (PostPRR-XLαs). Coimmunoprecipiation experiments and subsequent Western blot analyses using transfected HEK293T cells revealed that SNX9 could be immunoprecipiated with XLαs but not with Gsα or PostPRR-XLαs (Fig. 7*A*). We also performed similar coimmunoprecipitation experiments and found that neither Gsα nor the PostPRR-XLαs mutant was able to interact with Dnm1 and Dnm2 (Fig. 7 *B* and *C*). We then transfected HEK293T cells with cDNA encoding GFP-tagged

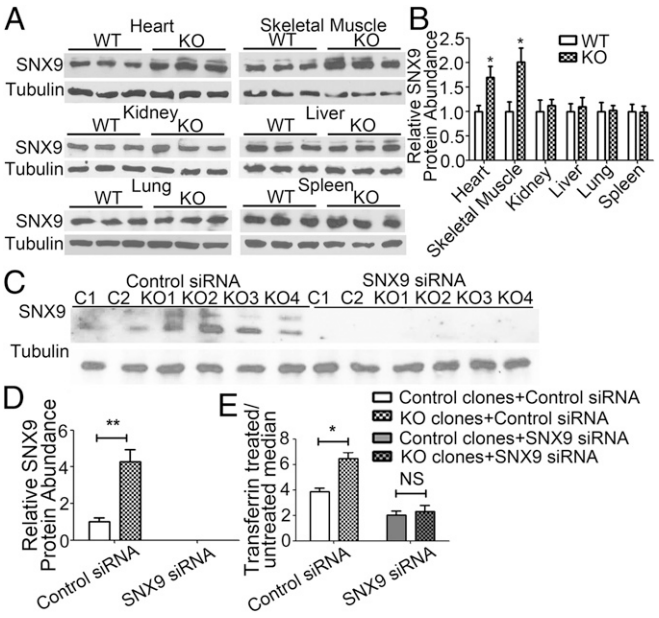

Fig. 6. Ablation of XLαs increases SNX9 expression, and suppression of SNX9 expression rescues the enhanced transferrin uptake in XLKO cells. (*A*) Protein lysates from P0 heart, skeletal muscle, kidney, liver, lung, and spleen were immunoblotted with SNX9 antibody. (*B*) Densitometric analysis of the relative abundances of SNX9 in different tissues. (*C*) Control and XLKO Ocy454 cells were transfected with siRNA directed against SNX9 or with control siRNA. Cell lysates were immunoblotted with SNX9 and α-tubulin antibodies. (*D*) Results from *C* were quantified by densitometry. Data represent mean ± SEM of at least three independent measurements; $*P < 0.05$. (*E*) siRNA transfected Ocy454 cells were untreated or treated with transferrin-Alexa Fluor 568 for 30 min, and then analyzed by flow cytometry for transferrin uptake. Data are mean ± SEM of three independent experiments ($n = 9–12$ per group); $*P < 0.05$, $**P < 0.01$.

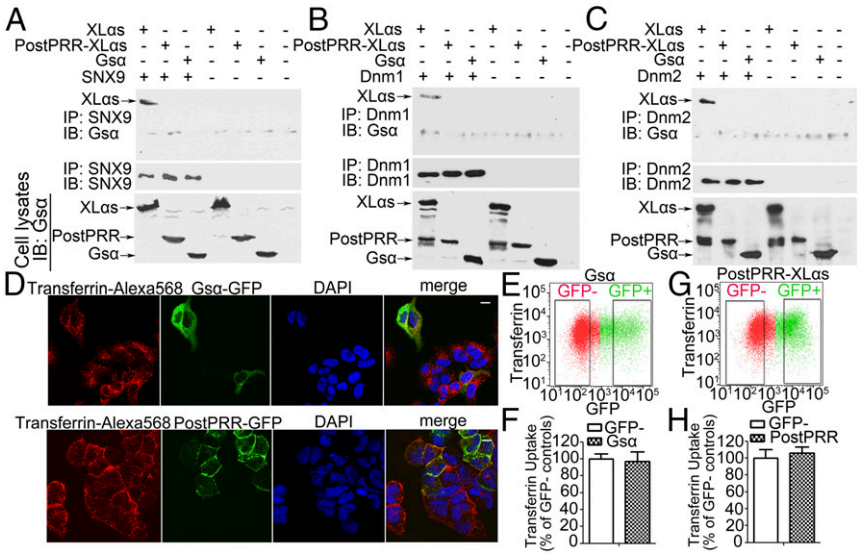

Fig. 7. Gsα and the XLαs mutant lacking the N-terminal region (PostPRR-XLαs) cannot interact with SNX9 or dynamins, or inhibit transferrin uptake. HEK293T cells were transfected with (*A*) SNX9, (*B*) Dnm1, or (*C*) Dnm2 plasmid, together with XLαs, PostPRR-XLαs, or Gsα plasmid, and the lysates of transfected cells were subjected to immunoprecipitation by using indicated antibodies. Subsequent immunoblots were performed by using the C-terminal anti-Gsα antibody, which could recognize XLαs, PostPRR-XLαs, and Gsα, as well as with (*A*) SNX9, (*B*) Dnm1, and (*C*) Dnm2 antibodies. Whole cell lysates were analyzed by using C-terminal anti-Gsα antibody to confirm successful transfection. Images are representative of three independent experiments. (*D*) Confocal microscopy analysis of HEK293T cells transiently expressing Gsα, or PostPRR-XLαs-GFP. (Scale bar, 10 μm.) (*E* and *G*) Representative plots of transferrin uptake in (*E*) Gsα-GFP and (*G*) PostPRR-XLαs-GFP transfected cells. (*F* and *H*) Quantification of the median values in GFP^+ and GFP^- cells. Data are mean ± SEM from three independent experiments ($n = 9$ per group).

Gsα or PostPRR-XLαs-GFP, and treated these cells with transferrin-Alexa Fluor 568 for 30 min. Confocal microscopy showed that transferrin was internalized in untransfected cells, as well as cells overexpressing Gsα or PostPRR-XLαs (Fig. 7*D*). Moreover, flow cytometry using transferrin-Alexa Fluor 568 revealed that, unlike XLαs, neither Gsα nor PostPRR-XLαs inhibited transferrin uptake in transfected HEK293T cells (Fig. 7 *E*–*H*).

Morphological Analysis of Coated Profiles in Cells Expressing Gsα and XLαs. Overexpression of dominant-negative dynamin mutants results in an increase in the percentage of clathrin-coated pits that have elongated necks (40). To determine whether XLαs overexpression alters clathrin-coated pit morphology, we performed transmission electron microscopy using HEK293T cells overexpressing GFP-tagged Gsα or GFP-tagged XLαs, which were incubated with 10 nm gold-conjugated transferrin for 1 h at 37 °C to aid in the identification of endocytic coated pits. Although gold-conjugated transferrin could be detected in internalized vesicles of both Gsα- and XLαs-overexpressing cells, the relative abundance of the differently shaped coated pits was significantly different (Fig. 8*A*). The majority of coated pits observed in Gsα-overexpressing cells were shallow (Fig. 8 *B* and *C*), with a smaller number of deep pits (Fig. 8 *D* and *E*) and few elongated pits identified, similar to the findings previously observed in untransfected or empty vector transfected cells (40). Overexpression of XLαs caused a pronounced shift in the ratio of shallow coated pits to deeply invaginated (Fig. 8 *F* and *G*) or elongated pits with long necks (Fig. 8 *H* and *I*).

Overexpression of XLαs Inhibits G Protein-Coupled Receptor Internalization. Clathrin-mediated endocytosis also mediates the agonist-induced internalization of GPCRs. It has been shown that XLαs can couple to multiple GPCRs including the PTH receptor (PTHR) (41, 42), which undergoes agonist-induced internalization (43). We treated HEK293T cells transfected with cDNA encoding PTHR and either GFP-tagged XLαs, GFP-tagged Gsα, or PostPRR-XLαs-GFP with tetramethylrhodamine-labeled PTH(1–34) (PTH-TMR) (10 nM), a PTHR agonist that has been previously utilized for monitoring the agonist-induced internalization of this receptor (44). Confocal microscopy showed that, 5 min after PTH stimulation, PTHR (as detected by the location of PTH-TMR) and Gsα were translocated into the intracellular space in Gsα-expressing cells (Fig. 9*A* and *SI Appendix*, Fig. S6*A*). PTHR also translocated into the intracellular region in PostPRR-XLαs–expressing cells, while the majority of PostPRR-XLαs, as shown previously (21), remained on the plasma membrane (Fig. 9*B*). In contrast, PTHR and XLαs-GFP signals were detectable only on the cell surface in XLαs-expressing cells (Fig. 9*C* and *SI Appendix*, Fig. S6*B*). Thus, the relative membrane/cytosol fluorescence intensity—for both red and green channels—was

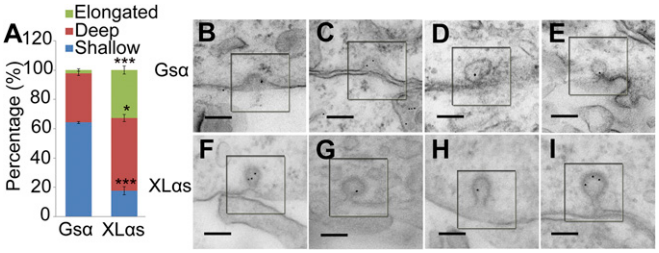

Fig. 8. Electron microscopy analysis of coated pit profiles in cells expressing Gsα or XLαs. (*A*) Quantification of the percentage of elongated, deep, and shallow pits in Gsα or XLαs overexpressing cells. A total of 39–45 pits were randomly selected per group for quantification. Shallow coated pits (C-shaped pits, not closing), deep coated pits (with short neck, the length of neck is smaller than the diameter of pit), and elongated pits (the length of neck is greater than the diameter of pit) were identified by their morphology and with the help of ImageJ software (NIH). The data shown are averages ± SEM of three independent experiments; $*P < 0.05$, $***P < 0.001$ vs. that in Gsα-expressing cells. (*B*–*I*) Representative coated pits from HEK293T cells overexpressing Gsα or XLαs. The images for Gsα group represent shallow pits (*B* and *C*) and deep pits (*D* and *E*). For XLαs group, *F* and *G* were scored as deep pits, while *H* and *I* were scored as elongated pits. (Scale bar, 100 nm.)

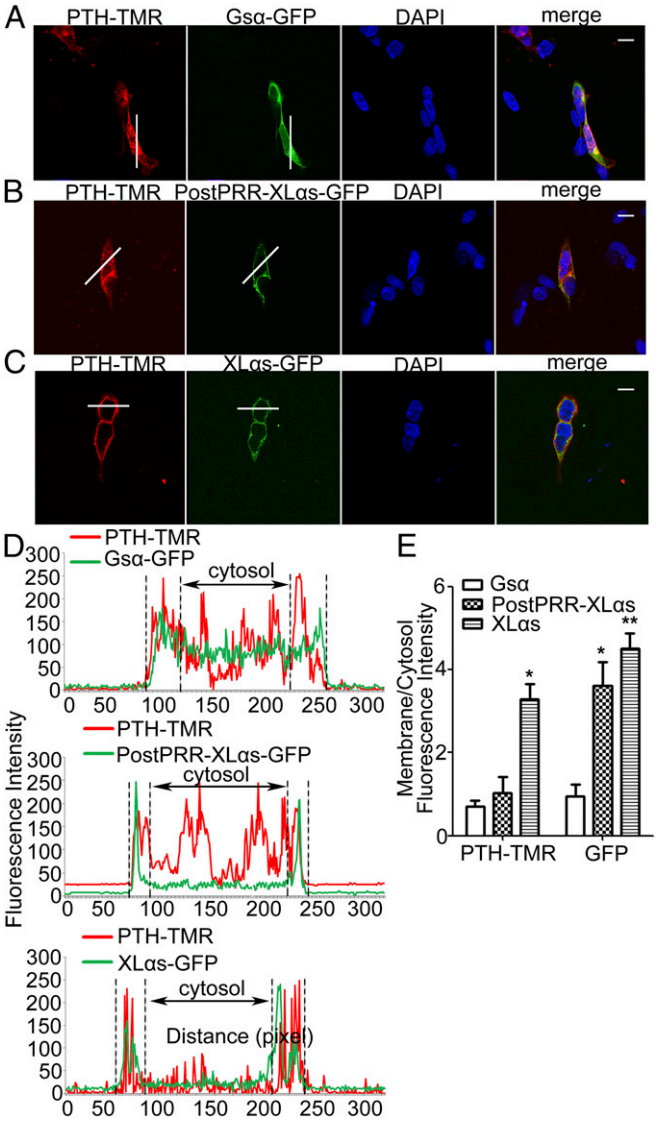

Fig. 9. Overexpression of XLαs prevents internalization of the G protein-coupled PTHR. (*A* and *B*) Confocal microscopy analysis of PTHR internalization in Gsα, XLαs, or PostPRR XLαs-overexpressing cells. PTHR was cotransfected with (*A*) Gsα-GFP, (*B*) PostPRR-XLas-GFP, or (*C*) XLas-GFP in HEK293T cells. The cells were treated for 5 min with PTH-TMR (10 nM), which internalizes the receptor. (Scale bar, 10 μm.) (*D*) Fluorescence intensities along the white lines in *A*–*C* were plotted as intensity histograms. *y* axis, intensity level; *x* axis, line distance. (*E*) Relative ratios of fluorescence intensity between plasma membrane and cytosolic area of PTHR and GFP were quantified by dividing the plasma membrane intensity to the cytosolic fluorescence intensity, using ImageJ. Data are mean ± SEM from 10 different cells. $*P < 0.05$, $**P < 0.01$.

significantly higher in XLαs-overexpressing cells compared with Gsα-overexpressing cells (Fig. 9 *D* and *E* and *SI Appendix*, Fig. S6 *C* and *D*).

We also employed total internal reflection fluorescence (TIRF) microscopy to monitor PTHR at the plasma membrane and quantify the effect of XLαs on PTHR internalization. HEK293 cells overexpressing dsRed-labeled PTHR and either Gαs-GFP or XLαs-GFP were treated with PTH(1–34), and the fluorescence intensity was monitored in live cells. In Gsα-expressing cells, PTH treatment led to diminished fluorescent intensity for both Gsα and PTHR (*SI Appendix*, Fig. S7 *A* and *B*), indicating that these proteins were internalized. In contrast, in XLαs-expressing cells the signal intensities remained constant despite PTH treatment, indicating that both XLαs and PTHR remained largely at the plasma membrane (*SI Appendix*, Fig. S7 *C* and *D*).

We then tested whether overexpression of XLαs affects internalization of the type 2 vasopressin receptor (V2R), another GPCR that internalizes via clathrin-mediated endocytosis (45, 46). HEK293T cells were cotransfected with XLαs-GFP and V2R cDNA and treated with tetramethylrhodamine-labeled vasopressin (VP-TMR) for 5 min. The cells cotransfected with Gsα-GFP and V2R cDNA were used as control. Confocal microscopy indicated a small degree of V2R internalization in XLαs-overexpressing cells, whereas most V2R signal was detected in the cytoplasmic portion of cells overexpressing Gsα (*SI Appendix*, Fig. S8).

To determine whether GPCR internalization is enhanced in the setting of XLαs ablation, we established primary cardiomyocyte cultures from WT and XLKO mice and subsequently transfected these cells with PTHR plasmid. We then treated these cells with PTH-TMR and performed fluorescence confocal microscopy. One minute after PTH-TMR treatment, most of the fluorescence signal appeared close to the plasma membrane in cells from WT mice, whereas a significant amount of signal appeared intracellular in cells from XLKO mice (*SI Appendix*, Fig. S9 *A*–*D*). While no differences were detected between XLKO and WT cells at 5 min (*SI Appendix*, Fig. S9 *E* and *F*), the subcellular distribution of PTH-TMR was significantly different between WT and XLKO cells at 15 min. WT cells displayed punctate intracellular fluorescence signal, whereas a significant portion of XLKO cells exhibited focal perinuclear spots (*SI Appendix*, Fig. S9 *G*–*I*). The latter pattern of subcellular distribution has been previously described for PTHR, indicating the localization of internalized PTHR at later stages (~30 min after ligand treatment) (47). In our experiments, most WT cells indeed displayed similar perinuclear spots 30 min following PTH-TMR treatment, although punctate fluorescence signal was also detectable. XLKO cells, on the other hand, showed markedly diminished fluorescence intensity but continued to have the focal perinuclear spots (*SI Appendix*, Fig. S9 *J* and *K*). These findings suggested that PTHR internalization was enhanced in the setting of XLαs deficiency.

Neither ALEX Nor the Gsα Portion Is Required for the Inhibitory Action of XLαs on Endocytosis. ALEX is translated from the XLαs transcript using a different ORF and can interact with XLαs (23). We generated an XLαs cDNA mutant in which the initiator methionine for ALEX was mutated to a threonine without changing the coding sequence for XLαs (ALEX(−)XLαs). A similar mutagenesis approach has previously been applied to successfully silence the translation of ALEX from rat XLαs cDNA (23). Confocal microscopy showed that both transferrin and PTHR internalization were inhibited in HEK293T cells transiently expressing ALEX(−)XLαs, similar to cells expressing native XLαs (*SI Appendix*, Fig. S10 *A* and *B*). By using flow cytometry, we also demonstrated that the degree of transferrin internalization was significantly lower in cells expressing ALEX(−)XLαs than in untransfected cells (*SI Appendix*, Fig. S10 *C* and *D*), thus indicating that ALEX does not a play a significant role in the action of XLαs in endocytosis.

We also examined a C-terminally truncated XLαs mutant (N-terminal XLαs), in which the portion containing the residues identical to Gsα are replaced with GFP. Confocal microscopy showed that this mutant was localized to the plasma membrane in most transfected HEK293T cells, although intracellular GFP signal was additionally detected in some cells (Fig. 10 *A* and *B*). Regardless, HEK293T cells expressing this mutant demonstrated significantly reduced transferrin uptake and PTHR internalization (Fig. 10 *A* and *B*). Flow cytometry also confirmed that N-terminal

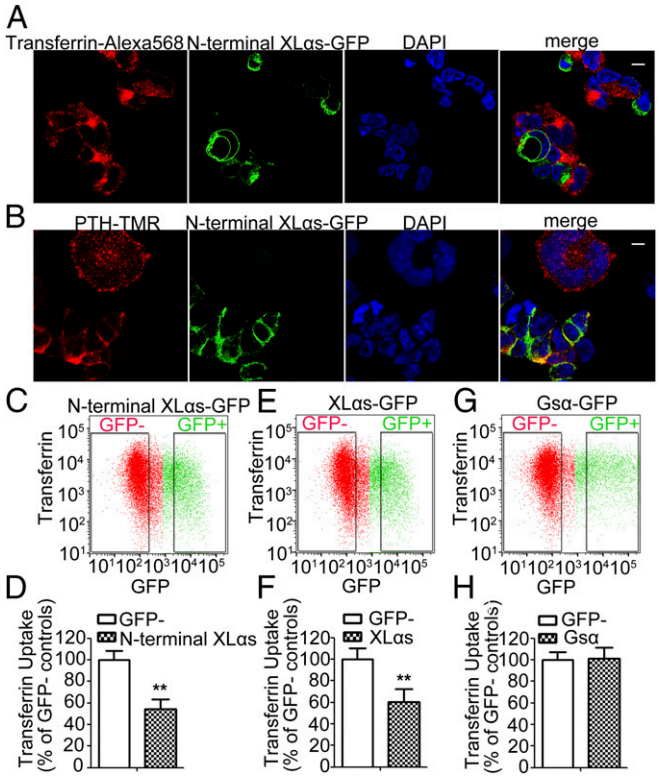

Fig. 10. N-terminal XLαs inhibits transferrin uptake and PTHR internalization. (*A*) Confocal microscopy analysis of N-terminal XLαs-GFP–expressing cells incubated with transferrin-Alexa Fluor 568 for 30 min. (*B*) Confocal microscopy analysis of PTHR internalization in N-terminal XLαs-GFP–expressing cells. (Scale bar, 10 μm.) Representative plots on transferrin uptake in (*C*) N-terminal XLαs-GFP, (*E*) XLαs-GFP, and (*G*) Gsα-GFP. (*D*, *F*, and *H*) Quantification of the median values of transferrin-Alexa Fluor 568 in GFP^+ and GFP^- cell populations. Data are mean ± SEM of two independent experiments ($n = 8$ per group). $^{**}P < 0.01$.

XLαs significantly inhibited transferrin uptake (Fig. 10 *C* and *D*). The degree of inhibition was similar to that for full-length XLαs (Fig. 10 *E* and *F*), while overexpression of Gsα did not inhibit transferrin uptake (Fig. 10 *G* and *H*). These results indicate that the Gsα portion of XLαs is not required for the inhibition of endocytosis.

Discussion

In this study, we identified SNX9 and dynamin as binding partners of the *GNAS*-derived imprinted G-alpha protein XLαs. Our investigations indicated that XLαs acts as an inhibitor of clathrin-mediated endocytosis independent of its Gsα-like actions. Accordingly, loss of XLαs enhanced the internalization of transferrin, which occurs via clathrin-mediated endocytosis, and resulted in increased iron uptake in cultured cells and in mice. Moreover, agonist-induced internalization of the G protein-coupled PTHR, which is also mediated by clathrin-mediated endocytosis, was more extensive in cells missing XLαs than in wild-type cells. These findings not only reveal a hitherto unknown cellular action for XLαs, but also provide insights into heterotrimeric G protein actions and the regulation of endocytosis.

Since endocytosis is key to multiple cellular processes, it is conceivable that ablation or overexpression of XLαs in our experiments led to secondary disruptions in certain cellular processes and, thereby, affected our results. However, evaluation of endocytosis as a primary readout is less likely to be confounded. It is unlikely that the enhanced transferrin uptake in XLKO Ocy454 cells and XLKO primary cardiomyocytes were secondary to basally increased TfRc levels, as we found that the TfRc mRNA levels were unaltered in those cells compared with WT cells. Likewise, increased TfRc levels cannot account for the increased iron uptake into the hearts of P10 XLKO pups, since the baseline TfRc mRNA abundance was diminished in XLKO hearts (~16% of WT). The reduction in TfRc mRNA in heart may reflect the increased tissue iron level at baseline, which was demonstrated by our histological analyses (Fig. 4*A*). Strikingly, these findings were obtained despite low serum iron levels in P10 XLKO pups. We are currently unable to offer any explanation for the latter finding, but it is tempting to speculate that the increased deposition of iron in heart and skeletal muscle might be responsible, at least partly, for the low circulating iron levels. Nonetheless, our additional findings obtained from XLKO neonates, which are affected minimally, if at all, by the postnatal defects involving multiple systems, clearly support the conclusion that XLαs plays a critical role in the regulation of tissue iron levels, consistent with an important action of XLαs in clathrin-mediated endocytosis.

The effect of XLαs on endocytosis is possibly through its interactions with SNX9 and dynamin, given that the N-terminally truncated XLαs mutant that is unable to interact with SNX9 or dynamins is also unable to inhibit endocytosis. SNX9 recruits dynamin to the plasma membrane and stimulates its oligomerization, thereby promoting its activity (48). Overexpression of dominant-negative dynamin mutants results in a dramatic increase in the number of pits with long necks (40). As indicated in our EM analyses, overexpression of XLαs also led to increased numbers of elongated pits relative to deep or shallow pits, consistent with the hypothesis that XLαs interferes with the actions of SNX9 and dynamin.

Since SNX9 knockdown rescues the enhanced internalization caused by XLαs deficiency in cultured cells, it appears that XLαs acts mechanistically upstream of SNX9. The increase in the protein level of SNX9 in XLαs-ablated cells and tissues may suggest that the interaction of XLαs with SNX9 contributes to the regulation of SNX9 levels, which is known to be critical for clathrin-mediated endocytosis (24, 33). Further studies are warranted to elucidate the precise mechanisms whereby XLαs mediates the action of SNX9.

Our experiments indicated that the interaction of XLαs with SNX9 and dynamin occurs via the portion of the XL domain including multiple proline-rich motifs and the highly conserved proline-rich domain. SNX9 contains an SH3 domain, which may mediate the interaction between this domain and SNX9. Consistent with this possibility, a 15-aa segment (GARRKIHLRPPSPEI) overlapping the conserved proline-rich region of human XLαs is predicted to interact with the SNX9 SH3 domain (according to MoDPepInt; modpepint.informatik.uni-freiburg.de) (49). Moreover, the proline-rich region comprises an evolutionarily conserved class I SH3 domain-binding motif (50). While a direct interaction seems likely, it remains possible that XLαs–SNX9 interaction occurs through another protein, and that these two are part of a larger complex, which also includes dynamin. Dynamin interacts with SNX9 via its own proline-rich lipid-binding domain and this interaction occurs via the SH3 domain of SNX9 (51). Considering that SNX9 forms homodimers via its BAR domain (52), it is tempting to speculate that XLαs and dynamin are brought together via interacting individually with SNX9. Future studies are needed to elucidate the molecular determinants of these interactions.

Considering that the XLαs transcript gives rise to both XLαs and ALEX, our transfection experiments using XLαs cDNA also led to ALEX overexpression. Likewise, the disruption of XLαs sequence is predicted to ablate not only XLαs but also ALEX in vivo. Thus, it is possible that ALEX may have mediated or contributed to the interaction of XLαs with SNX9 and/or dynamin and the effect of XLαs on endocytosis. However, our mutational analyses using transfected cells suggested that ALEX,

which was shown to interact with XLαs (23), is not required for the inhibitory action of XLαs on endocytosis.

XLαs is able to mediate basal and GPCR-activated cAMP generation when overexpressed (21, 41, 53). Interestingly, our previous findings have suggested that XLαs promotes basal and GPCR-activated IP3 generation in mouse kidney and cultured cells (30). It could thus be argued that the effect of XLαs on endocytosis is secondary to the activation of these signaling pathways. However, this possibility is unlikely, since endocytosis was not inhibited as a result of Gsα overexpression, which, like XLαs overexpression, enhances basal cAMP signaling (42). Moreover, C-terminal truncation of XLαs leading to the loss of its Gα portion did not abolish the inhibitory action of XLαs in endocytosis. In some transfected HEK293 cells, this truncation mutant (N-terminal XLαs) localized to intracellular sites, as well as the plasma membrane. Similarly, an XLαs construct using the rat XL domain has previously been studied and was shown to localize exclusively to the plasma membrane in transfected PC12 cells but not in COS7 cells, in which localization was detected in additional subcellular compartments (22). Thus, it is possible that the Gsα portion of XLαs contributes to the plasma membrane localization of XLαs and may function concurrently with other cell-specific mechanisms.

Genetic mutations in humans and studies of different mouse models implicate loss of XLαs activity, by itself or combined with loss of Gsα activity, in a number of disorders, including intrauterine growth retardation, heterotopic ossification, platelet defects, and disrupted glucose and energy metabolism with increased central sympathetic outflow (18, 54–56). It has also been shown that XLαs hyperactivity contributes to the pathogenesis of breast cancers associated with increased chromosome 20q copy number (20). Diseases caused by XLαs alterations could thus result, at least partly, from changes in clathrin-mediated endocytosis. In addition, studies have revealed that SNX9 plays additional roles in membrane trafficking and actin dynamics, thus contributing to a wide range of cellular processes, including clathrin-independent endocytosis, cell division, and tumor metastasis (57). Since our study strongly suggests that XLαs acts as a regulator of SNX9 activity or levels, it appears likely that altered XLαs function also affects these other SNX9-dependent cellular events.

The Gsα portion seems to be unnecessary for the XLαs-mediated inhibition of endocytosis. It thus appears unlikely that this action of XLαs is impaired due to inactivating mutations located within the Gsα portion (such as those found in patients with pseudopseudohypoparathyroidism, who carry paternal *GNAS* mutations), unless the mutation causes diminished XLαs expression as a result of nonsense-mediated decay or protein instability. The same mutations, however, impair the G protein signaling action of XLαs (42). Selective effects of these *GNAS* mutations on the different actions of XLαs would have implications in the associated clinical phenotypes.

The modest increase of Gsα levels in XLKO cells is concordant with a previous study demonstrating elevated Gsα levels, as well as agonist-induced cAMP production, in XLKO renal brush border membranes (30). This mechanism governing the XLKO-induced elevation in Gsα levels remain unknown. Nonetheless, it is unlikely that the elevated Gsα levels contribute to the increased transferrin uptake observed in XLKO cells, as our findings argue against a role for Gsα overexpression in endocytosis.

In summary, our findings indicate that XLαs plays a role as an inhibitor of clathrin-mediated endocytosis, and that this role of XLαs is upstream of SNX9 and independent of its G protein signaling action. Consistent with this cellular action, loss of XLαs results in increased transferrin uptake and iron accumulation in cultured cells and mice.

Methods

Expression Plasmids. Plasmids encoding SNX9, Dnm1, Dnm2, Dnm1K44A-GFP, and Dnm2K44A-GFP were obtained from Addgene. cDNA encoding FLAG-tagged XLαs, HA-tagged PostPRR-XLαs, HA-tagged Gsα, XLαs, and Gsα with GFP tag were described previously (21, 58). The plasmid encoding PostPRR-XLαs-GFP was constructed by substituting the sequences encoding PostPRR-XLαs for the full-length XLαs in the XLαs-GFP construct. ALEX(–)XLαs-GFP plasmid was constructed by point mutation at ALEX start codon region in the XLαs-GFP construct. The plasmid encoding N-terminal XLαs-GFP was constructed by inserting the N-terminal XLαs portion into pcDNA3.1/CT-GFP TOPO vector using CT-GFP Fusion TOPO Expression Kit (Thermo Fisher Scientific). The plasmid encoding the PTHR–dsRed fusion protein, PTHR, and Vasopressin Type 2 Receptor (V2R) were reported before (21, 59).

Mice. XLKO mice were generated by disrupting the first exon encoding XLαs on the paternal allele (26). These mice were maintained in a CD1 genetic background. All of the animal experiments were conducted in accordance with the accepted standards of the Institutional Animal Care and Use Committee, and the studies were approved by the Massachusetts General Hospital (MGH) Subcommittee on Research Animal Care.

Mass Spectrometry. C3H10T1/2 cells were transfected with FLAG-tagged XLαs or YFP, and the cell lysates were purified by anti-FLAG affinity resin and followed by LC-MS/MS analysis. LC-MS/MS was carried out at the Taplin Biological Mass Spectrometry Facility, Cell Biology Department, Harvard Medical School.

Cell Culture and Transfection. Primary cardiomyocytes were prepared from P2 mouse hearts as previously described, and cultured in Ham's F-10 medium with 10% horse serum and 5% FBS at 37 °C (60). HEK293T cells were cultured in DMEM with 10% FBS at 37 °C, while osteocytic cell line Ocy454 cells were maintained in α-minimum essential medium with 10% FBS at 33 °C (27, 28). Primary cardiomyocytes were transiently transfected by using Lipofectamine LTX & PLUS (Invitrogen). HEK293T cells were transiently transfected by using either Lipofectamine 2000 (Invitrogen) for endocytic vesicle profiling by EM, or PolyJet (SignaGen Laboratories) for all other assays.

Generation of XLαs Knockout Ocy454 Cells by CRISPR/Cas9. Three different guide RNAs targeting XLαs were designed through the sgRNA Designer website (Broad Institute), and cloned into pSpCas9(BB)-2A-GFP vector (Addgene) (*SI Appendix*, Table S2). The osteocytic Ocy454 cells were transfected with the plasmids containing XLαs sgRNAs, and 3 d following transfection, successful delivery of sgRNA plasmids was confirmed by visualizing green fluorescent protein expression by fluorescence microscopy. Transfected cells were sorted using fluorescence-activated cell sorting (FACS), and individual GFP-positive cells were cloned into 96-well plates and allowed to expand for 3 wk. Successful knockout of XLαs in single cloned Ocy454 cells were assessed by Western blot analysis and sequencing of DNA fragments covering the sgRNA target region (*SI Appendix*, Fig. S2 and Table S3).

Cell Lysis, Immunoprecipitation, and Western Blot Analysis. HEK293T cells were lysed by using HNTG lysis buffer (20 mm Hepes, pH 7.4, 150 mm NaCl, 10% glycerol, 1% Triton X-100, 1.5 mm $MgCl_2$, 1.0 mm EGTA) containing Complete Protease inhibitor mixture tablets (Roche). For immunoprecipitations, equal amounts of cell lysate were incubated with the indicated antibodies for 16–18 h at 4 °C with rotation. Protein A/G-agarose beads (Santa Cruz Biotechnology) were then added to the lysates to capture the immune complex for 1 h. After washing with HNTG buffer four times and PBS one time, the immune complexes were eluted from the beads by boiling in 2× SDS sample buffer. For immunoblot analysis, cell lysates and immunoprecipitated proteins were resolved by 10% SDS-polyacrylamide gel electrophoresis (SDS/PAGE) and transferred to nitrocellulose membranes (Bio-Rad). Western blots were then incubated with specific antibodies. Antibody against FLAG was purchased from Sigma. Antibodies against SNX9, Dnm1, and Dnm2 were from Santa Cruz Biotechnology. Polyclonal antiserum against mouse XLαs was described previously (61). Gsα antibody, which recognizes Gsα, XLαs, and PostPRR-XLαs, was purchased from Millipore. L-Ferritin antibody was purchased from Novus Biologicals.

Confocal Microscopy. HEK293T cells were cotransfected with GFP-tagged XLαs or Gsα, together with PTHR or V2R plasmids. Forty-eight hours after transfection, the cells were washed three times with 10 mM Hepes pH 7.5 with 0.1% BSA and then treated with PTH-TMR (10 nM) or VP-TMR (1 μm) for 5 min at 37 °C to visualize internalization of PTHR and V2R. Primary cardiomyocytes from P2 WT and XLKO mice were transfected with PTHR plasmid, and treated with PTH-TMR (10 nM) for 1 min, 5 min, 15 min, or 30 min at room temperature. PTH-TMR was synthesized at the MGH Biopolymer Core facility, and

VP-TMR was described previously (62). For transferrin receptor internalization, HEK293T cells transfected with XLαs-GFP or Gsα-GFP were serum starved for 1 h and treated with transferrin-Alexa Fluor 568 (Thermo Fisher Scientific) (10 μg/mL) for 30 min. Cells were washed three times with cold PBS and fixed with 4% paraformaldehyde (PFA) in PBS for 20 min. HEK293T cells cotransfected with HA-tagged Gsα or PostPRR-XLαs were treated with PTH-TMR (10 nM) for 5 min. After fixation with 4% PFA for 20 min, cells were permeabilized with 0.2% Triton X-100 in PBS and subsequently incubated for 30 min with a blocking solution containing 0.2% Triton X-100, 1% BSA, and 5% goat serum in PBS. Cells were then immunoreacted to a rabbit anti-HA antibody (Santa Cruz Biotechnology), followed by Alexa Fluor 488-conjugated donkey anti-rabbit IgG (Life Technologies). Fluorescent intensity was visualized and analyzed with a Zeiss LSM 510 Confocal Microscope (Ragon Institute) and Zeiss Zen software. To quantify the fluorescence intensity ratio between the plasma membrane and cytosol in XLαs-GFP or Gsα-GFP transfected cells, a line was drawn across each one of the cells. The line intensity profiles were obtained by using ImageJ software, as described (63, 64). The results shown are averages ± SEM from 10 different cells from at least three independent experiments.

TIRF Microscopy. TIRF microscopy analysis of PTHR internalization was performed as previously described (21). Briefly, HEK293T cells were cultured on FluoroDish (World Precision Instruments, Inc.) and transiently transfected with cDNA encoding Gαs-GFP or XLαs-GFP, as well as PTHR-dsRed. Forty-eight hours after transfection, cells were stimulated with 10 nM PTH(1–34) and fluorescent signal intensities in individual live cells with the brightest GFP signal were analyzed by a TIRF objective over 50 min.

Flow Cytometric Analysis for Transferrin Uptake and Apoptosis. For transferrin uptake assay, HEK293T cells were transfected with Gαs-GFP, XLαs-GFP, PostPRR-XLαs-GFP, Dnm1K44A-GFP, or Dnm2K44A-GFP. Forty-eight hours after transfection, cells were serum starved for 1 h and subsequently incubated with transferrin-Alexa Fluor 568. Thirty minutes after the addition of transferrin-Alexa Fluor 568, the transfected HEK293T cells, Ocy454 cells, and primary cardiomyocytes isolated from P2 mice were washed with PBS and dissociated from the culture plates. Cells were then subjected to flow cytometry by using FACSAriaII (BD Biosciences) at MGH Center for Regenerative Medicine Flow Cytometry Core. The results were analyzed by FlowJo software for the median values of transferrin uptake in GFP-positive and GFP-negative cell populations.

For apoptosis analysis in primary cardiomyocytes with iron overload, the cells were treated with or without 150, 300, 600 μM $FeCl_3$ as previously described (33). After 72 h of incubation, the cells were gently detached by 0.05% Trypsin-EDTA (Invitrogen) and stained with Annexin V-FITC Apoptosis Detection Kit (Abcam), and Annexin V-positive/PI-negative cells were gated by flow cytometric assay to quantify the apoptotic cell number.

cDNA Synthesis and qRT-PCR Analysis. Total RNA was prepared using the RNeasy Plus Mini Kit (QIAGEN). One microgram of total RNA was used to synthesize first-strand cDNA using ProtoScript II First-Strand cDNA Synthesis Kit (New England Biolabs). qRT-PCR analysis was performed with specific primers and FastStart Universal SYBR Green Master (Roche) with β-actin as a reference gene. Primers used for qRT-PCR were: β-actin (F) GATCTGGCACCACACCTTCT and (R) GGGGTGTTGAAGGTCTCAAA; TfRc (F) ATGCCCTCTCTGGTGACATTTGGA and (R) ACCCTCCACAAGCACACTCTTTCT; and XLαs (F) CTCATCGACAAGCAACTGGA and (R) CCCTCTCCGTTAAACCCATT.

In Vivo Iron-Loading Experiments. Iron dextran was injected i.p. daily (400 mg per kilogram body weight per day) for a total duration of 10 d starting from neonatal age, i.e., P0–P9. Mice injected with vehicle (0.9% sodium chloride solution) were used as control. Mice were killed at P10 for the analysis. Hearts were removed and fixed in 4% PFA and embedded in paraffin (MGH Center for Skeletal Research). The 5-μm sections were stained with Iron Stain Kit (Sigma) using staining protocol recommended by the manufacturer. The deposition of iron was visualized as blue depositions using a bright field microscope. For heart tissues with vehicle injection, a modified diaminbenzidine-enhanced Perls' stain containing cobalt chloride was used (65).

Iron Analysis. Serum iron and tissue nonheme iron concentrations were determined as described previously (66). Tissue iron is reported as micrograms of iron per gram of wet weight tissue.

Transmission Electron Microscopy. HEK293T cells were transfected with XLαs-GFP or Gsα-GFP plasmids for 48 h. The percentage of GFP-positive cells was determined to assess the transfection efficiency, and over 95% cells were GFP-positive. Cells were incubated with transferrin 10 nm gold conjugate (Cytodiagnostics) in PBS supplemented with 1 mM $MgCl_2$, 1 mM $CaCl_2$, 5 mM glucose, and 0.2% BSA for 1 h, and then washed and fixed with 2.5% glutaraldehyde/2% PFA in 0.1 M cacodylate buffer (pH 7.4) for 2 h at room temperature. Cells were then processed for thin-section electron microscopy using a Tecnai G2 Spirit Bio TWIN electron microscope (FEI Company) at the Harvard Medical School EM facility.

Statistical Analysis. The means ± SEM of multiple independent measurements were calculated. The unpaired two-tailed Student's *t* test was used to determine the significance of differences between means. *P* values smaller than 0.05 ($*P < 0.05$, $**P < 0.01$, $***P < 0.001$) were considered to be significant.

ACKNOWLEDGMENTS. We thank Dr. Gavin Kelsey (Babraham Institute) for kindly providing the XLKO mice. This work was supported in part by grants from NIH/National Institute of Diabetes and Digestive and Kidney Diseases (NIDDK) (R01DK073911 to M.B.) and NIH/National Institute of Arthritis and Musculoskeletal and Skin Diseases (NIAMS) (5K08AR067285 to M.N.W. and R01AR05965 to P.D.P.). Q.H. is supported by NIH/NIDDK Grant T32DK007028. R.B. is supported by NIH Grant DK096586 and University of Baltimore Maryland Polycystic Kidney Disease Core Center Grant P30DK090868. Histology analyses were performed at the Massachusetts General Hospital Endocrine Unit Center for Skeletal Research, Bone Cell and Signaling Core, funded by Grant P30AR066261 from NIH/NIAMS.

1. Doherty GJ, McMahon HT (2009) Mechanisms of endocytosis. *Annu Rev Biochem* 78: 857–902.
2. McMahon HT, Boucrot E (2011) Molecular mechanism and physiological functions of clathrin-mediated endocytosis. *Nat Rev Mol Cell Biol* 12:517–533.
3. Elkin SR, Lakoduk AM, Schmid SL (2016) Endocytic pathways and endosomal trafficking: A primer. *Wien Med Wochenschr* 166:196–204.
4. Kumari S, Mg S, Mayor S (2010) Endocytosis unplugged: Multiple ways to enter the cell. *Cell Res* 20:256–275.
5. Nesbit MA, et al. (2013) Mutations in AP2S1 cause familial hypocalciuric hypercalcemia type 3. *Nat Genet* 45:93–97.
6. Züchner S, et al. (2005) Mutations in the pleckstrin homology domain of dynamin 2 cause dominant intermediate Charcot-Marie-Tooth disease. *Nat Genet* 37:289–294.
7. Bitoun M, et al. (2005) Mutations in dynamin 2 cause dominant centronuclear myopathy. *Nat Genet* 37:1207–1209.
8. Harold D, et al. (2009) Genome-wide association study identifies variants at CLU and PICALM associated with Alzheimer's disease. *Nat Genet* 41:1088–1093.
9. Nixon RA (2005) Endosome function and dysfunction in Alzheimer's disease and other neurodegenerative diseases. *Neurobiol Aging* 26:373–382.
10. Bareford LM, Swaan PW (2007) Endocytic mechanisms for targeted drug delivery. *Adv Drug Deliv Rev* 59:748–758.
11. Oldham WM, Hamm HE (2008) Heterotrimeric G protein activation by G-protein-coupled receptors. *Nat Rev Mol Cell Biol* 9:60–71.
12. Weinstein LS, Liu J, Sakamoto A, Xie T, Chen M (2004) Minireview: GNAS: Normal and abnormal functions. *Endocrinology* 145:5459–5464.
13. Turan S, Bastepe M (2015) GNAS spectrum of disorders. *Curr Osteoporos Rep* 13: 146–158.
14. Weinstein LS, Chen M, Liu J (2002) Gs(alpha) mutations and imprinting defects in human disease. *Ann N Y Acad Sci* 968:173–197.
15. Kehlenbach RH, Matthey J, Huttner WB (1994) XL alpha s is a new type of G protein. *Nature* 372:804–809.
16. Hayward BE, Moran V, Strain L, Bonthron DT (1998) Bidirectional imprinting of a single gene: GNAS1 encodes maternally, paternally, and biallelically derived proteins. *Proc Natl Acad Sci USA* 95:15475–15480.
17. Shore EM, et al. (2002) Paternally inherited inactivating mutations of the GNAS1 gene in progressive osseous heteroplasia. *N Engl J Med* 346:99–106.
18. Richard N, et al. (2013) Paternal GNAS mutations lead to severe intrauterine growth retardation (IUGR) and provide evidence for a role of XLαs in fetal development. *J Clin Endocrinol Metab* 98:E1549–E1556.
19. Izzi B, et al. (2012) Methylation defect in imprinted genes detected in patients with an Albright's hereditary osteodystrophy like phenotype and platelet Gs hypofunction. *PLoS One* 7:e38579.
20. Garcia-Murillas I, et al. (2014) An siRNA screen identifies the GNAS locus as a driver in 20q amplified breast cancer. *Oncogene* 33:2478–2486.
21. Liu Z, Turan S, Wehbi VL, Vilardaga JP, Bastepe M (2011) Extra-long Galphas variant XLalphas protein escapes activation-induced subcellular redistribution and is able to provide sustained signaling. *J Biol Chem* 286:38558–38569.
22. Pasolli HA, Klemke M, Kehlenbach RH, Wang Y, Huttner WB (2000) Characterization of the extra-large G protein alpha-subunit XLalphas. I. Tissue distribution and subcellular localization. *J Biol Chem* 275:33622–33632.
23. Klemke M, Kehlenbach RH, Huttner WB (2001) Two overlapping reading frames in a single exon encode interacting proteins–A novel way of gene usage. *EMBO J* 20: 3849–3860.

24. Soulet F, Yarar D, Leonard M, Schmid SL (2005) SNX9 regulates dynamin assembly and is required for efficient clathrin-mediated endocytosis. *Mol Biol Cell* 16:2058–2067.
25. Urrutia R, Henley JR, Cook T, McNiven MA (1997) The dynamins: Redundant or distinct functions for an expanding family of related GTPases? *Proc Natl Acad Sci USA* 94: 377–384.
26. Plagge A, et al. (2004) The imprinted signaling protein XL alpha s is required for postnatal adaptation to feeding. *Nat Genet* 36:818–826.
27. Spatz JM, et al. (2015) The Wnt inhibitor sclerostin is up-regulated by mechanical unloading in osteocytes in Vitro. *J Biol Chem* 290:16744–16758.
28. Wein MN, et al. (2015) HDAC5 controls MEF2C-driven sclerostin expression in osteocytes. *J Bone Miner Res* 30:400–411.
29. Pignolo RJ, et al. (2011) Heterozygous inactivation of Gnas in adipose-derived mesenchymal progenitor cells enhances osteoblast differentiation and promotes heterotopic ossification. *J Bone Miner Res* 26:2647–2655.
30. He Q, Zhu Y, Corbin BA, Plagge A, Bastepe M (2015) The G protein alpha subunit variant XLalphas promotes inositol 1,4,5-trisphosphate signaling and mediates the renal actions of parathyroid hormone in vivo. *Sci Signal* 8:ra84.
31. Papanikolaou G, Pantopoulos K (2005) Iron metabolism and toxicity. *Toxicol Appl Pharmacol* 202:199–211.
32. Oudit GY, et al. (2004) Taurine supplementation reduces oxidative stress and improves cardiovascular function in an iron-overload murine model. *Circulation* 109: 1877–1885.
33. Chen MP, Cabantchik ZI, Chan S, Chan GC, Cheung YF (2014) Iron overload and apoptosis of HL-1 cardiomyocytes: Effects of calcium channel blockade. *PLoS One* 9: e112915.
34. Zecca L, Youdim MB, Riederer P, Connor JR, Crichton RR (2004) Iron, brain ageing and neurodegenerative disorders. *Nat Rev Neurosci* 5:863–873.
35. Enns CA (2001) Pumping iron: The strange partnership of the hemochromatosis protein, a class I MHC homolog, with the transferrin receptor. *Traffic* 2:167–174.
36. Fernandez-Rebollo E, et al. (2012) Loss of XLalphas (extra-large alphas) imprinting results in early postnatal hypoglycemia and lethality in a mouse model of pseudohypoparathyroidism Ib. *Proc Natl Acad Sci USA* 109:6638–6643.
37. Krechowec SO, et al. (2012) Postnatal changes in the expression pattern of the imprinted signalling protein XLalphas underlie the changing phenotype of deficient mice. *PLoS One* 7:e29753.
38. Ma MP, Chircop M (2012) SNX9, SNX18 and SNX33 are required for progression through and completion of mitosis. *J Cell Sci* 125:4372–4382.
39. Kay BK, Williamson MP, Sudol M (2000) The importance of being proline: The interaction of proline-rich motifs in signaling proteins with their cognate domains. *FASEB J* 14:231–241.
40. Damke H, Binns DD, Ueda H, Schmid SL, Baba T (2001) Dynamin GTPase domain mutants block endocytic vesicle formation at morphologically distinct stages. *Mol Biol Cell* 12:2578–2589.
41. Bastepe M, et al. (2002) Receptor-mediated adenylyl cyclase activation through XLalpha(s), the extra-large variant of the stimulatory G protein alpha-subunit. *Mol Endocrinol* 16:1912–1919.
42. Linglart A, et al. (2006) Coding GNAS mutations leading to hormone resistance impair in vitro agonist- and cholera toxin-induced adenosine cyclic 3′,5′-monophosphate formation mediated by human XLalphas. *Endocrinology* 147:2253–2262.
43. Huang Z, Chen Y, Nissenson RA (1995) The cytoplasmic tail of the G-protein-coupled receptor for parathyroid hormone and parathyroid hormone-related protein contains positive and negative signals for endocytosis. *J Biol Chem* 270:151–156.
44. Ferrandon S, et al. (2009) Sustained cyclic AMP production by parathyroid hormone receptor endocytosis. *Nat Chem Biol* 5:734–742.
45. Bouley R, et al. (2013) Heterologous downregulation of vasopressin type 2 receptor is induced by transferrin. *Am J Physiol Renal Physiol* 304:F553–F564.
46. Feinstein TN, et al. (2013) Noncanonical control of vasopressin receptor type 2 signaling by retromer and arrestin. *J Biol Chem* 288:27849–27860.
47. Conway BR, et al. (2001) Quantitative analysis of agonist-dependent parathyroid hormone receptor trafficking in whole cells using a functional green fluorescent protein conjugate. *J Cell Physiol* 189:341–355.
48. Lundmark R, Carlsson SR (2004) Regulated membrane recruitment of dynamin-2 mediated by sorting nexin 9. *J Biol Chem* 279:42694–42702.
49. Kundu K, Mann M, Costa F, Backofen R (2014) MoDPepInt: An interactive web server for prediction of modular domain-peptide interactions. *Bioinformatics* 30:2668–2669.
50. Ferraro E, Peluso D, Via A, Ausiello G, Helmer-Citterich M (2007) SH3-Hunter: Discovery of SH3 domain interaction sites in proteins. *Nucleic Acids Res* 35:W451–W454.
51. Lundmark R, Carlsson SR (2003) Sorting nexin 9 participates in clathrin-mediated endocytosis through interactions with the core components. *J Biol Chem* 278: 46772–46781.
52. Yarar D, Surka MC, Leonard MC, Schmid SL (2008) SNX9 activities are regulated by multiple phosphoinositides through both PX and BAR domains. *Traffic* 9:133–146.
53. Klemke M, et al. (2000) Characterization of the extra-large G protein alpha-subunit XLalphas. II. Signal transduction properties. *J Biol Chem* 275:33633–33640.
54. Shore EM, Kaplan FS (2010) Inherited human diseases of heterotopic bone formation. *Nat Rev Rheumatol* 6:518–527.
55. Freson K, et al. (2008) GNAS defects identified by stimulatory G protein alpha-subunit signalling studies in platelets. *J Clin Endocrinol Metab* 93:4851–4859.
56. Xie T, et al. (2006) The alternative stimulatory G protein alpha-subunit XLalphas is a critical regulator of energy and glucose metabolism and sympathetic nerve activity in adult mice. *J Biol Chem* 281:18989–18999.
57. Bendris N, Schmid SL (2017) Endocytosis, metastasis and beyond: Multiple facets of SNX9. *Trends Cell Biol* 27:189–200.
58. Aydin C, et al. (2009) Extralarge XL(alpha)s (XXL(alpha)s), a variant of stimulatory G protein alpha-subunit (Gs(alpha)), is a distinct, membrane-anchored GNAS product that can mimic Gs(alpha). *Endocrinology* 150:3567–3575.
59. Bouley R, et al. (2005) Downregulation of the vasopressin type 2 receptor after vasopressin-induced internalization: Involvement of a lysosomal degradation pathway. *Am J Physiol Cell Physiol* 288:C1390–C1401.
60. Patten RD, et al. (2004) 17beta-estradiol reduces cardiomyocyte apoptosis in vivo and in vitro via activation of phospho-inositide-3 kinase/Akt signaling. *Circ Res* 95: 692–699.
61. Liu Z, et al. (2011) Transgenic overexpression of the extra-large Gsalpha variant XLalphas enhances Gsalpha-mediated responses in the mouse renal proximal tubule in vivo. *Endocrinology* 152:1222–1233.
62. Chen S, et al. (2011) Visualizing microtubule-dependent vasopressin type 2 receptor trafficking using a new high-affinity fluorescent vasopressin ligand. *Endocrinology* 152:3893–3904.
63. Ueda H, Fujita R, Yoshida A, Matsunaga H, Ueda M (2007) Identification of prothymosin-alpha1, the necrosis-apoptosis switch molecule in cortical neuronal cultures. *J Cell Biol* 176:853–862.
64. Armstrong S, Pereverzev A, Dixon SJ, Sims SM (2009) Activation of P2X7 receptors causes isoform-specific translocation of protein kinase C in osteoclasts. *J Cell Sci* 122: 136–144.
65. Canali S, et al. (2017) Endothelial cells produce bone morphogenetic protein 6 required for iron homeostasis in mice. *Blood* 129:405–414.
66. Zumbrennen-Bullough KB, et al. (2014) MicroRNA-130a is up-regulated in mouse liver by iron deficiency and targets the bone morphogenetic protein (BMP) receptor ALK2 to attenuate BMP signaling and hepcidin transcription. *J Biol Chem* 289: 23796–23808.